

Exciton diffusion and annihilation in nanophotonic Purcell landscapes

T. V. Raziman,[†] C. Peter Visser,[†] Shaojun Wang,^{†,‡} Jaime Gómez Rivas,[†] and
Alberto G. Curto^{*,†}

[†]*Department of Applied Physics and Institute for Photonic Integration, Eindhoven
University of Technology, Eindhoven, The Netherlands*

[‡]*MOE Key Laboratory of Modern Optical Technologies and Jiangsu Key Laboratory of
Advanced Optical Manufacturing Technologies, School of Optoelectronic Science and
Engineering, Soochow University, Suzhou 215006, China*

E-mail: A.G.Curto@TUE.nl, Phone: +31-40-247-4205

Abstract

Excitons spread through diffusion and interact through exciton-exciton annihilation. Nanophotonics can counteract the resulting decrease in light emission. However, conventional enhancement treats emitters as immobile and non-interacting. It neglects exciton redistribution between regions with different enhancements and the increase in non-radiative decay at high exciton densities. Here, we go beyond the localized Purcell effect to exploit exciton dynamics and turn their typically detrimental impact into additional emission. As interacting excitons diffuse through optical hotspots, the balance of excitonic and nanophotonic properties leads to either enhanced or suppressed photoluminescence. We identify the dominant enhancement mechanisms in the limits of high and low diffusion and annihilation. Diffusion lifts the requirement of spatial overlap between excitation and emission enhancements, which we harness to maximize

emission from highly diffusive excitons. In the presence of annihilation, we predict improved enhancement at increasing powers in nanophotonic systems dominated by emission enhancement. Our guidelines are relevant for efficient and high-power light-emitting diodes and lasers tailored to the rich dynamics of excitonic materials such as monolayer semiconductors, perovskites, or organic crystals.

Introduction

Nanophotonics can improve light emission by enhancing excitation and radiative rates, and beaming radiation^{1–13}. In the conventional Purcell effect, emitters such as molecules and quantum dots are treated as localized point dipoles^{14,15}. Total enhancement thus benefits from the product of excitation and emission at a point, which guides the design of nano-resonators and metamaterials made of metals and dielectrics.

For excitonic emitters, however, the picture of emission arising from non-interacting dipoles at fixed positions is incomplete. In a variety of semiconductors, excitons are mobile and spread to large diffusion lengths compared to nanophotonic scales (10 – 500 nm). Examples include perovskites (diffusion length $L_D \sim 100 - 1000$ nm)^{16–18}, monolayer transition metal dichalcogenides (hundreds of nm)^{19,20}, quantum dots (tens of nm)^{21,22}, organic crystals (1 – 100 nm for singlet excitons, 10 – 1000 nm for triplets)²³, and carbon nanotubes (hundreds of nm)^{24,25}. As a result, excitons can emit far from the intense near field where they originate, affecting their radiative rate. Additionally, diffusion deteriorates emission as emitters approach defects and boundaries, where they might decay non-radiatively^{26–29}. A photonic modification of the radiative decay rate could decrease the effective diffusion length, thus improving performance.

Another important aspect of exciton dynamics is exciton-exciton annihilation^{25,30,31}. At high exciton densities, this nonlinear process contributes to and even dominates non-radiative losses, degrading the performance of light-emitting devices at high powers^{32,33} and potentially preventing lasing. Annihilation thus curtails the advantages of nanophotonic intensity

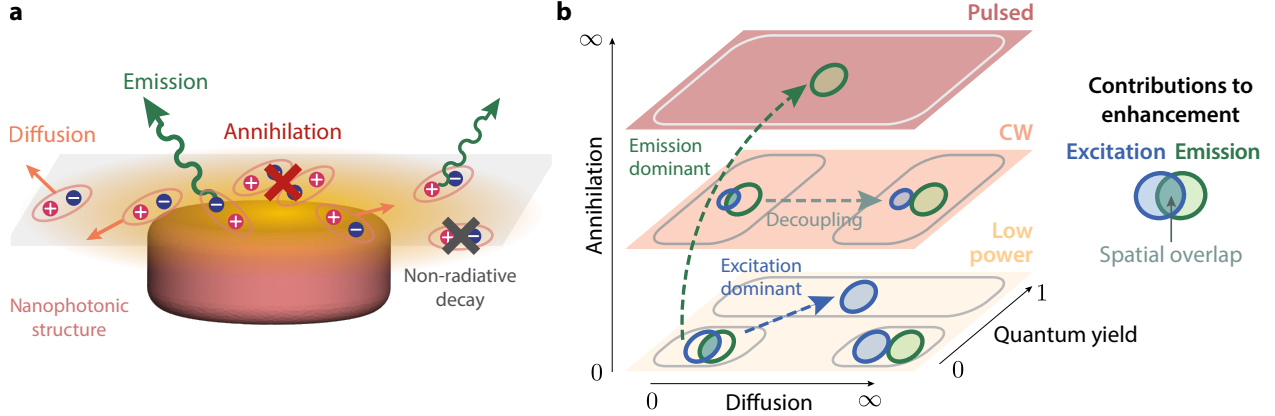


Figure 1: Impact of exciton dynamics on nanophotonic emission enhancement. (a) Excitation and emission of a thin excitonic film (gray) above an array of nanodisks in the presence of diffusion and annihilation. Excitation enhancement (orange cloud) generates excitons that diffuse (orange arrows), annihilate (red), or decay non-radiatively (black) before radiative decay (green). (b) Contributions to the total photoluminescence enhancement of excitation, emission, and their spatial overlap (see Table 1). Limiting cases of diffusion, annihilation, and quantum yield with qualitatively similar enhancement behaviors are grouped into common areas. At low power, diffusion lifts the requirement of spatial overlap between excitation and emission enhancements for emitters with low quantum yield, whereas enhancement with high quantum yield is independent of diffusion or emission enhancement. At high power, the benefit of excitation enhancement decreases and even vanishes for continuous-wave and pulsed illuminations, with emission dominating the total enhancement. For continuous-wave illumination, enhancement depends on diffusion but is independent of quantum yield; for pulsed illumination, enhancement does not depend on quantum yield or diffusion.

enhancement as well by simultaneously increasing non-radiative decay.

Here, we analyze the interplay of exciton dynamics and nanophotonic enhancement for thin films of excitonic emitters in nanostructured landscapes. We provide analytical results for enhancement under limiting cases of exciton dynamics. We demonstrate that, although diffusion and annihilation typically impede nanophotonic enhancement, it is possible to design nanostructures to overcome the lost efficiency. Diffusion can increase photoluminescence by taking excitons to highly radiative locations when excitation and emission are spatially decoupled. Radiative rate enhancement can ameliorate the loss of efficiency arising from annihilation, while the interplay between annihilation and diffusion can improve performance by redistributing the local exciton density. In summary, a careful balance of the relative strengths and spatial overlap of excitation and emission enhancements is the key to effi-

cient excitonic-nanophotonic systems. Our guidelines for tailoring nanophotonic structures to diffusing and annihilating excitons will aid the design of efficient light-emitting devices.

Results

Exciton dynamics and nanophotonic enhancement

Excitons evolve in nanophotonic environments under the combined influence of incident intensity, radiative enhancement, non-radiative decay, diffusion, and annihilation (Figure 1a). We consider excitonic emitters in ultrathin films on top of nanodisk arrays with a negligible variation of electromagnetic fields across the film thickness. The two-dimensional exciton density evolves according to the exciton dynamics equation²⁰:

$$\frac{\partial n(\mathbf{r}, t)}{\partial t} = I(\mathbf{r}, t)\sigma - [\Gamma_r(\mathbf{r}) + \Gamma_{nr,0}]n(\mathbf{r}, t) + D\nabla^2 n(\mathbf{r}, t) - \gamma n^2(\mathbf{r}, t), \quad (1)$$

where $n(\mathbf{r}, t)$ is the exciton density at point \mathbf{r} at time t , I is the nanophotonically enhanced local excitation intensity at \mathbf{r} , σ is the absorption coefficient, $\Gamma_r(\mathbf{r})$ is the spatially varying radiative decay rate, $\Gamma_{nr,0}$ is the intrinsic non-radiative decay rate, D is the diffusion constant, and γ is the annihilation constant. In the absence of nanophotonic structures, the intrinsic decay rates are $\Gamma_{r,0} = \eta_0\Gamma_0$ and $\Gamma_{nr,0} = (1 - \eta_0)\Gamma_0$, where Γ_0 is the total decay rate and η_0 is the intrinsic quantum yield. The exciton decay time is $\tau_0 = 1/\Gamma_0$ and the diffusion length is $L_D = \sqrt{D\tau_0}$. We assume that the nanostructures do not modify the non-radiative decay rate $\Gamma_{nr,0}$ and the diffusion constant D , although our model can incorporate such changes as well. We also neglect saturation of absorption at high power.

To compare systems with different excitonic and nanophotonic properties and extract the universal behavior of nanophotonic systems in the presence of exciton dynamics, we non-dimensionalize Equation (1). We identify physically relevant scales of exciton density, incident power, length, and time in the system to scale the variables n , I , \mathbf{r} , and t with these values:

- $n' = n/n_0$, where $n_0 = \Gamma_0/\gamma$ is the exciton density at which $\Gamma_0 n$ (the intrinsic total decay, which includes radiative and non-radiative rates but not annihilation) equals γn^2 (the density-dependent annihilation),
- $I' = I/I_0$, where $I_0 = \Gamma_0 n_0/\sigma$ is the incident continuous-wave power at which $I\sigma$ (the exciton generation) equals $\Gamma_0 n_0$ (the intrinsic decay at $n = n_0$),
- $\mathbf{r}' = \mathbf{r}/P$, where P is the period of the nanophotonic structures,
- $t' = t/\tau_0$, where τ_0 is the exciton decay time.

The characteristic scales depend on both excitonic and nanophotonic properties. Note that we perform scaling with respect to intrinsic properties (in the absence of nanostructures), except the length scale, which is the period of the array. Expressing Equation (1) in terms of the primed variables, we obtain the non-dimensionalized exciton dynamics equation

$$\frac{\partial n'(\mathbf{r}', t')}{\partial t'} = F_{ex}(\mathbf{r}')I'(t') - F_{decay}(\mathbf{r}', \eta_0)n'(\mathbf{r}', t') + D'\nabla'^2 n'(\mathbf{r}', t') - n'^2(\mathbf{r}', t'), \quad (2)$$

where F_{ex} and F_{em} are the local nanophotonic excitation and radiative rate enhancements, and $F_{decay} = \eta_0 F_{em} + 1 - \eta_0$ is the localized total decay rate enhancement. The non-dimensionalized diffusion constant $D' = D\tau_0/P^2$ is related to the diffusion length and the period of the nanophotonic structures by $D' = (L_D/P)^2$. The annihilation rate γ does not appear explicitly and is part of the characteristic incident power $I' = I\gamma\sigma/\Gamma_0^2$, demonstrating the utility of non-dimensionalization in comparing different systems. Excitonic materials that differ only in the annihilation rate γ will behave identically in a nanophotonic system except for scaling of incident power. We perform electromagnetic simulations using the surface integral equation (SIE) method and solve the non-dimensionalized exciton dynamics equation (2) to demonstrate the impact of exciton diffusion and annihilation on nanophotonic photoluminescence enhancement. We illustrate the diverse behavior and the possible scenarios of exciton dynamics using a variety of nanostructures.

First, we analyze how diffusion affects it by spreading excitons out. We study excitonic emitters consisting of orientationally averaged dipoles above an array of silicon nanodisks.

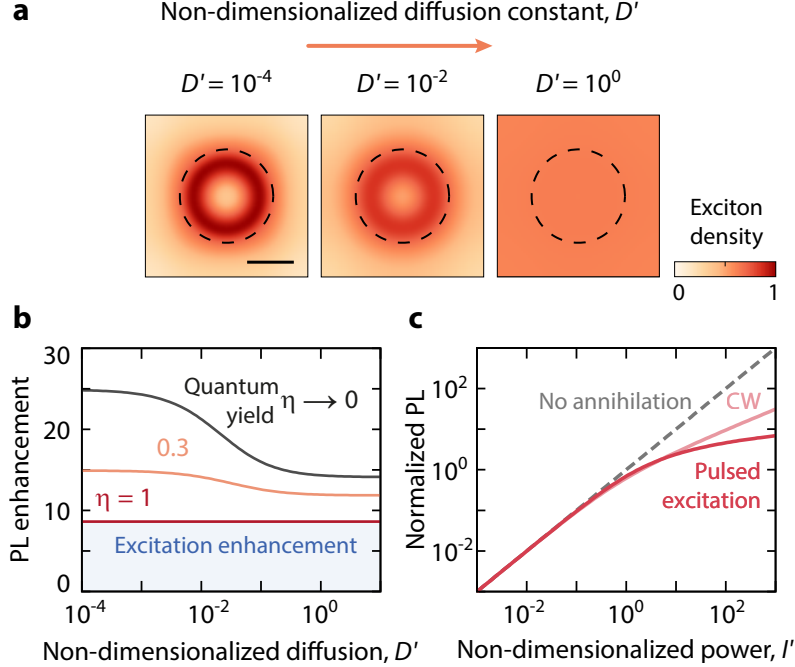


Figure 2: Exciton diffusion and annihilation usually lead to reduced photoluminescence. (a) Exciton density of emitters with intrinsic quantum yield $\eta_0 = 1$ above an array of silicon nanodisks with radius $R = 100$, height $H = 75$, and period $P = 365$ nm. A low-power, continuous plane wave is incident from below the disks at $\lambda = 553$ nm. Scale bar 100 nm. (b) The nanophotonic photoluminescence enhancement of the nanodisk array decreases due to diffusion. The blue area indicates enhancement due to excitation only. (c) In the absence of nanophotonic structures, photoluminescence scales sublinearly with incident power due to annihilation.

Although exciton density and diffusion are two-dimensional because the exciton film is thin, the exciton dipole moment can have components out of the plane – therefore, we average the orientations in all three dimensions³⁴. We assume perfect collection efficiency of the emission. We illuminate with a continuous-wave source at low power so that annihilation is initially negligible.

For low diffusion constants, the exciton density concentrates near the edge of the nanodisk, corresponding to the local excitation profile of an electric dipole in the nanodisk (Figure 2a). As the non-dimensionalized diffusion constant D' increases, the exciton density distribution expands, eventually becoming uniform over the unit cell. In this case, diffusion suppresses the total photoluminescence enhancement by taking excitons from regions of

high radiative enhancement to positions of low enhancement (Figure 2b). The total photoluminescence is a combination of excitation and emission enhancements. Immobile emitters with low intrinsic quantum yield benefit from both excitation and emission enhancements, whereas only the increased excitation is relevant for emitters with high quantum yield^{35,36}. The Purcell effect can be strongly modified upon diffusion, while the excitation is unaffected by diffusion in the absence of saturation effects. The impact of diffusion is the strongest for emitters with low quantum yield because of their larger contribution from radiative enhancement. For emitters with high intrinsic quantum yield, the Purcell effect enhances only the decay rate and not the photoluminescence. Diffusion reduces this enhancement (Supporting Figure S1a).

In the absence of nanostructures, exciton-exciton annihilation suppresses photoluminescence by opening an additional non-radiative channel at high excitation powers and exciton densities (Figure 2c). Compared to continuous-wave excitation, pulsed excitation creates higher instantaneous exciton densities, thereby reducing emission even further. Nanophotonic structures can ameliorate this deterioration of emission, as we shall discuss later. Additionally, the quick initial decay due to the high exciton density shortens the decay time considerably (Supporting Figure S1b).

Enhancing emission through diffusion

Generally, the deterioration of nanophotonic enhancement with diffusion is due to losing the advantage of spatial overlap between excitation and emission enhancements. To understand the contribution of each process and their overlap, we solve the non-dimensionalized exciton dynamics equation (2) analytically for limiting cases of quantum yield, diffusion, and annihilation (Supporting Section S1). We list the photoluminescence enhancement for these extremes in Table 1 and depict the contributions from excitation and emission and their overlap in Figure 1b, where the levels indicate the increasing role of annihilation. When the incident power is much lower than $I_0 = \Gamma_0 n_0 / \sigma$, annihilation is negligible compared to

Table 1: Nanophotonic photoluminescence enhancement (F_{tot}) in the presence of exciton dynamics: limiting cases of diffusion, quantum yield, and incident power. $\langle x \rangle$ represents the spatial average of the quantity x in the unit cell. Spatial averages of products of excitation and emission enhancements such as $\langle F_{ex} \cdot F_{em} \rangle$ indicate the benefit of their spatial overlap. Diffusion decouples the enhancements spatially, turning the expressions into products of spatial averages such as $\langle F_{ex} \rangle \langle F_{em} \rangle$.

Diffusion	Quantum yield	Incident power (with annihilation)		
		$I' \rightarrow 0$	$I' \rightarrow \infty$	
			Continuous	Pulsed
$D' = 0$	$\eta_0 \rightarrow 0$	$\langle F_{ex} \cdot F_{em} \rangle$	$\langle \sqrt{F_{ex}} \cdot F_{em} \rangle$	$F_{tot} = \langle F_{em} \rangle$
	$\eta_0 = 1$	$\langle F_{ex} \rangle$		
$D' \rightarrow \infty$	$\eta_0 \rightarrow 0$	$\langle F_{ex} \rangle \langle F_{em} \rangle$	$\langle \sqrt{F_{ex}} \rangle \langle F_{em} \rangle$	
	$\eta_0 = 1$	$\langle F_{ex} \rangle$		

intrinsic decay (bottom level in Figure 1b). In this regime of negligible annihilation ($I' \rightarrow 0$) and diffusion length much smaller than the period ($D' \rightarrow 0$), the total enhancement for emitters with poor efficiency ($\eta_0 \rightarrow 0$) is $\langle F_{ex}(\mathbf{r}) \cdot F_{em}(\mathbf{r}) \rangle$, which is the spatial average of the product of local enhancements in the unit cell. Hence, in the absence of diffusion, we obtain high total enhancement if the excitation and emission significantly overlap.

In the regime of high diffusion, however, the total enhancement becomes $\langle F_{ex}(\mathbf{r}) \rangle \langle F_{em}(\mathbf{r}) \rangle$, which is the product of the average values of excitation and emission in the unit cell. The spatial overlap of the enhancement factors is then no longer of benefit. As a result, the photoluminescence enhancement typically worsens with diffusion for low-efficiency emitters (Figure 3a). Although emitters with high quantum yield do not suffer a similar loss of enhancement because their emission efficiency does not change, their decay rate deteriorates with increasing diffusion (Figure 3a). Surprisingly, diffusion can modify the decay rate of emitters even in the limit of zero quantum yield (Supporting Figure S2).

Diffusion can also improve emission by removing the spatial overlap between enhancement contributions. By controlling the excitation conditions such as the angle of incidence, polarization, or wavelength, we can lift the requirement of spatial overlap for maximum photoluminescence. As a first example, we spatially decouple excitation and emission by

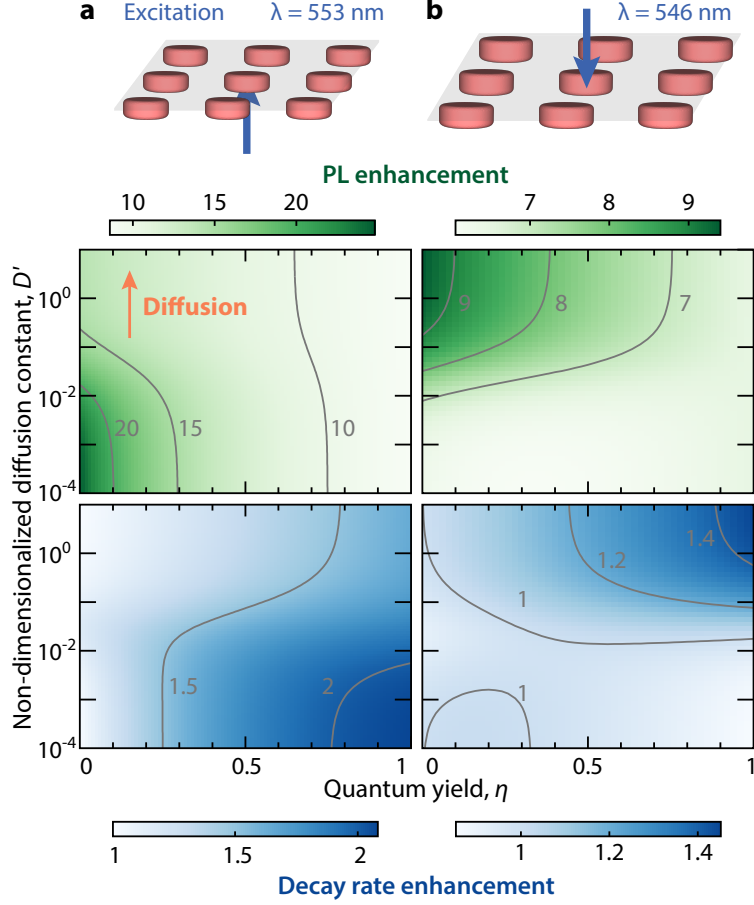


Figure 3: Diffusion can both improve or degrade photoluminescence depending on the nanophotonic system. Photoluminescence and total decay rate enhancements under low-power, pulsed illumination of excitons above arrays of silicon nanodisks: (a) illuminated from below with $R = 100$, $H = 75$, $P = 365$ nm; (b) illuminated from above with $R = 120$, $H = 90$, $P = 445$ nm. In gray, contours of constant enhancement with their respective values. Excitation and emission wavelengths are equal.

exploiting the angular pattern of emission in an array with a different geometry (Figure 3b and Supporting Figure S3). The excitation profile shows a strong front-back asymmetry because the high refractive index of silicon causes retardation of electromagnetic fields along its height⁵. We illuminate the nanodisks from above to benefit from this asymmetry. The photoluminescence increases with diffusion at low η_0 , and so does the decay rate enhancement at high η_0 . Nanostructures designed under the assumption of immobile emitters can thus behave differently with diffusing excitons. Whether the impact of diffusion on enhancement is beneficial or detrimental depends on the nanophotonic system. Nanostructures aiming at

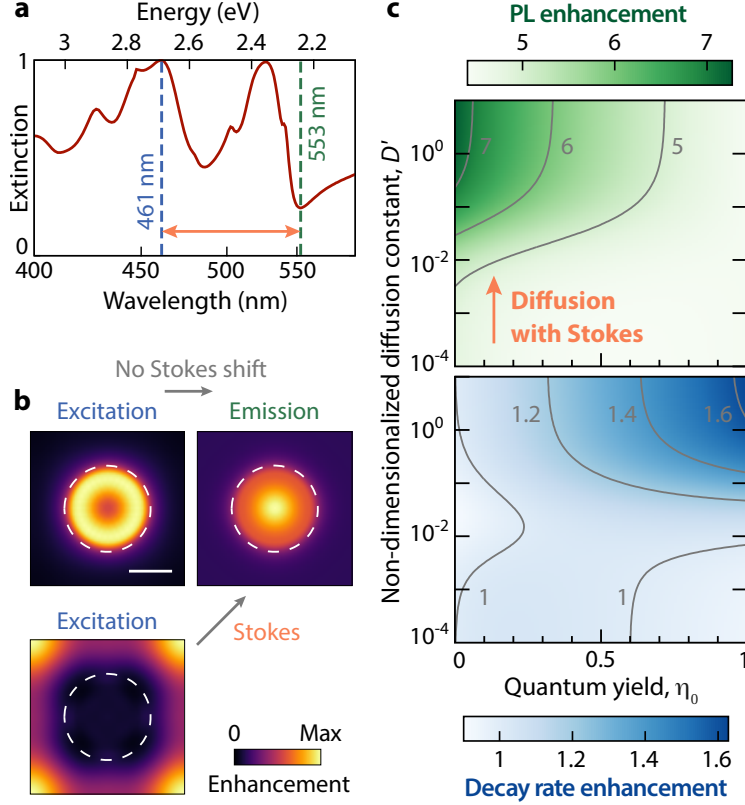


Figure 4: A Stokes shift can decouple excitation and emission enhancements at different wavelengths to improve photoluminescence through diffusion. (a) Extinction spectrum of the array of silicon nanodisks in Figure 3a with multiple resonances. (b) The maps of excitation and emission enhancements at $\lambda_{em} = 553$ nm overlap significantly. Changing the excitation wavelength to 461 nm decouples the excitation enhancement at λ_{ex} from the emission at λ_{em} . Scale bar 100 nm. (c) Enhancements of photoluminescence and total decay rate under excitation at λ_{ex} and emission at λ_{em} including the Stokes shift above.

maximum output from excitonic materials should thus take diffusion into account due to their spatially dependent enhancements^{4,7,37,38}.

As a second case of enhancement through diffusion, we exploit the Stokes shift between excitation and emission wavelengths to decouple them spatially. We utilize the diversity of resonances supported by arrays of silicon nanodisks. (Figure 4a). For zero detuning with emission and excitation at $\lambda_{em} = \lambda_{ex} = 553$ nm, the excitation and radiative enhancements are both strongest above the disk (Figure 4b). The exciton density is highest near the edge because of the relatively high excitation enhancement there (Figure 2a). Due to the spatial overlap between enhancements, diffusion decreases photoluminescence as it transports

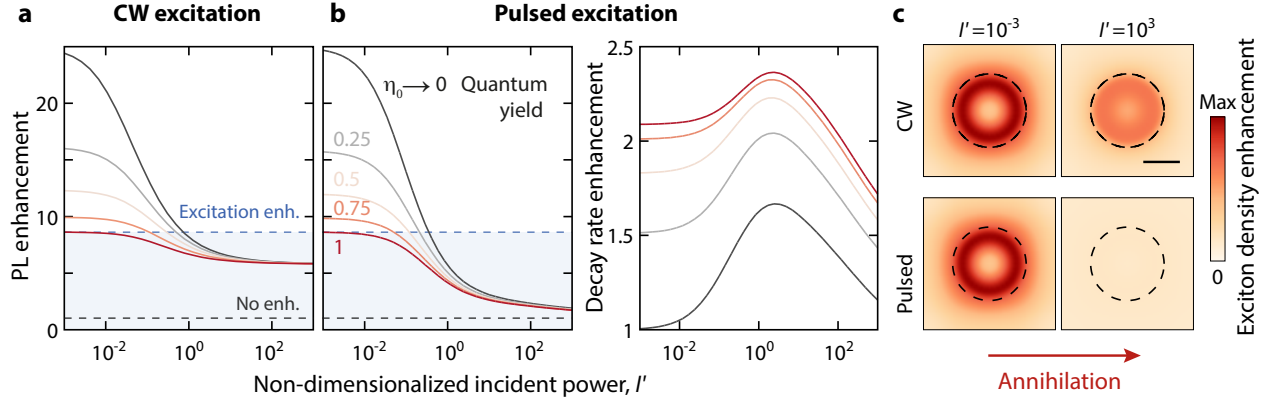


Figure 5: Exciton-exciton annihilation typically suppresses photoluminescence enhancement at increasing excitation powers. (a) Photoluminescence enhancement for the array of silicon nanodisks in Figure 3a as a function of incident power under continuous-wave illumination. Blue and gray lines denote the levels of excitation enhancement and no enhancement. (b) Enhancement of photoluminescence and total decay rate under pulsed illumination. (c) Change in exciton density enhancement averaged over time with increasing incident power.

excitons from regions of high excitation to areas of low radiative enhancements (Figure 3a). However, if the excitonic material has a Stokes shift between excitation at $\lambda_{ex} = 461$ and emission at $\lambda_{em} = 553$ nm, the excitation enhancement is almost completely decoupled from the emission enhancement (Figure 4b). Diffusion thus takes the excitons generated at λ_{ex} to regions of high radiative enhancement at λ_{em} , improving photoluminescence and decay rate compared to immobile excitons (Figure 4c). Emitters typically have a Stokes shift between excitation and emission, giving us a handle to turn diffusion to our advantage.

Overcoming annihilation through nanophotonic enhancement

So far, we have only considered the effects of diffusion on nanophotonic enhancement. Next, we add exciton-exciton annihilation, which typically suppresses photoluminescence. As the incident power of a continuous-wave source increases, photoluminescence enhancement usually decreases for all quantum yields in the absence of diffusion (Figure 5a for the array in Figure 3a). At high power, the total nanophotonic enhancement falls even below the excitation enhancement (blue line). Exciton-exciton annihilation increases nonlinearly with power, suppressing the effect of excitation enhancement and reducing the steady-state exci-

ton density enhancement (Figure 5c). At low power, the photoluminescence enhancement is due to F_{ex} for high- η_0 emitters, whereas it arises from the product of F_{ex} and F_{em} for low- η_0 emitters. In contrast, at high power, the photoluminescence enhancement is the product of $\sqrt{F_{ex}}$ and F_{em} independent of the quantum yield because exciton-exciton annihilation becomes the dominant non-radiative decay channel (Table 1).

The suppression of photoluminescence is even stronger for pulsed excitation (Figure 5b), where annihilation neutralizes the excitation enhancement completely as manifest in the time-averaged exciton density (Figure 5c). The emission enhancement still results in increased photoluminescence compared to the bare emitters. Exciton density enhancement on the nanostructure modifies the total decay rate via exciton-exciton annihilation, although the effect is neutralized once again at very high incident power (Figure 5b).

Diffusion can alleviate part of the detrimental effects of annihilation by smearing the hotspots of exciton density. Although emitters with high intrinsic quantum yield have diffusion-independent photoluminescence enhancement at low incident power (Figure 4c), the drop in enhancement with increasing power is much slower for highly diffusing excitons (Figure 6a).

Next, we demonstrate that it is possible to improve performance even as annihilation becomes dominant. At low incident power, high- η_0 emitters benefit only from excitation enhancement whereas at high power, the effect of excitation diminishes and emission enhancement becomes dominant (Table 1). Therefore, nanophotonic structures with emission enhancement comparable to or higher than excitation enhancement offer improved photoluminescence enhancement with increasing power. This counter-intuitive behavior arises from the increasing benefit of emission enhancement as a strong non-radiative decay channel opens at high exciton densities. We exemplify such a case with an array of silver nanoparticles which has significantly higher emission enhancement compared to excitation enhancement (Supporting Figure S4). Indeed, as the incident power increases, emitters above the array of silver nanoparticles benefit from increasing photoluminescence enhancement. (Figure 6b).

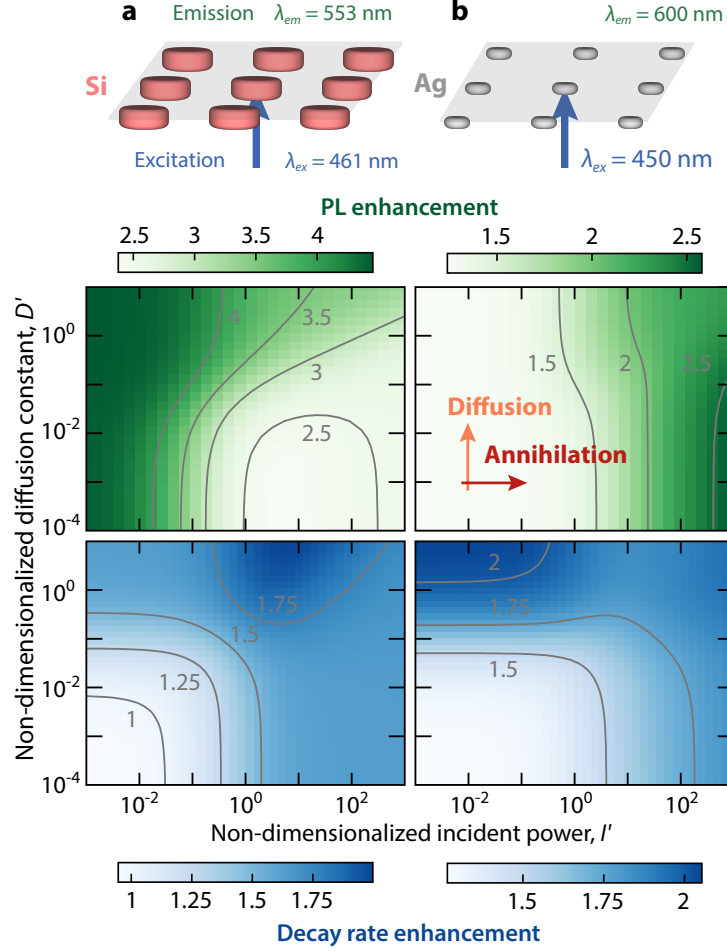


Figure 6: Interplay between nanophotonic properties, annihilation, and diffusion. Increasing incident power can either decrease or increase nanophotonic emission enhancement. (a,b) Geometry, photoluminescence enhancement under continuous-wave illumination, and total decay rate enhancement under pulsed illumination, for emitters with $\eta_0 = 1$ above: (a) silicon nanodisks with $R = 100$, $H = 75$, $P = 365$ nm; (b) silver nanodisks with $R = 50$, $H = 40$, $P = 350$ nm.

Although we have shown improved performance here for plasmonic nanoparticles, dielectric nanostructures with strong emission enhancements behave similarly (Supporting Figure S5). High- η_0 emitters with exciton-exciton annihilation are important for light-emitting devices, which suffer from efficiency loss at high powers. The ability to reduce the impact of annihilation on emission through the combination of nanophotonic design and diffusion is thus of practical interest.

Nanophotonic enhancement in relevant excitonic materials

Finally, we show that the non-dimensionalized limits of diffusion and annihilation become significant for light emission from realistic excitonic emitters. We tabulate reported excitonic parameters for representative materials and calculate their characteristic exciton density n_0 , incident power I_0 and the non-dimensionalized diffusion constant D' (Supporting Table S1). For transition metal dichalcogenide monolayers and two-dimensional perovskites, D' is of the order of unity. As a result, the excitons spread through the entire unit cell before they decay. Monolayer semiconductors with low quantum yield thus benefit from additional enhancement in nanostructures designed for diffusive excitons (Supporting Figure S6). Emitters with high quantum yield also suffer from strong annihilation. The incident power at which annihilation becomes dominant, I_0 , is very low (of the order of $\text{nW}/\mu\text{m}^2 - \mu\text{W}/\mu\text{m}^2$), especially for transition metal dichalcogenides (Supporting Table S1). As a result, they benefit from additional enhancement in nanophotonic systems designed for materials with high annihilation (Supporting Figure S7).

Although we focused our analysis on excitons in thin films, the general principles also apply to other geometries. Nanowires support one-dimensional diffusion and can be placed along directions of high excitation and emission enhancements to obtain stronger photoluminescence (Supporting Figure S10). In the case of thick excitonic materials around nanophotonic structures, exciton diffusion will be three-dimensional, and the decay of the evanescent near field away from the nanostructure plane will also play a role. In addition to photonic enhancement, material interfaces can modify intrinsic decay, diffusion, and annihilation through doping, dielectric screening, or phonons^{29,33,39-43}. Our model can accommodate such effects through the use of locally varying excitonic parameters modified by the environment. It is also possible to prevent such environmental modification of excitonic parameters with a thin dielectric spacer. At high exciton densities in transition metal dichalcogenide monolayers, exciton-phonon effects modify diffusion, resulting in halo formation⁴⁴⁻⁴⁶. Making the diffusion constant dependent on the exciton density⁴⁴ in the exciton dynamics equation

can model such behavior. Some materials show superdiffusive behavior where the exciton density spreads faster than the prediction from linear diffusion. A rate equation model can describe such behavior by making the diffusion constant dependent on time or exciton density^{47,48}. In materials such as organic semiconductors where there are multiple varieties of excitons, incorporating their interconversion into the rate equation can identify effects such as negative diffusion⁴⁹. Additional phenomena could further exploit diffusion to improve performance. Diffusion spreads the excitons away from the nanostructures, where Ohmic losses in the nanophotonic system are stronger. The reduction of absorption losses could therefore further contribute to total enhancement due to diffusion. Analogous to annihilation, saturation effects at higher excitation powers can suppress the enhancement⁵⁰ and could be similarly overcome through diffusion. On the other hand, designing nanophotonic systems with extremely high emission enhancements can counteract the effect of diffusion by reducing the lifetime and thus the diffusion length (Supporting Figure S9). Last, applying strain on monolayer semiconductors can result in exciton funneling, the directional transport of excitons towards regions of high strain^{38,51-54}. Using nanostructures as sources of both strain and nanophotonic enhancement promises a new direction to control light-matter interaction.

Conclusion

We have combined exciton dynamics and nanophotonics to illustrate the range of scenarios beyond the conventional Purcell effect for photoluminescence enhancement in the presence of diffusion and annihilation. Although usually detrimental for light emission, careful nanophotonic design can turn diffusion into an advantage and partly mitigate the detrimental effect of exciton-exciton annihilation. We presented analytical expressions of enhancement for the limiting regimes of diffusion and annihilation to formulate the conditions for improved exciton photoluminescence. Removing the spatial overlap between excitation and emission

enhancements can improve emission from diffusive excitons in nanostructured landscapes – for instance, by including a Stokes shift between excitation and emission wavelengths. Similar decoupling is possible through other strategies such as excitation and emission at different angles. It is also possible to alleviate the detrimental effects of exciton-exciton annihilation by tuning the relative strengths of excitation and emission enhancements and by capitalizing on diffusion to reduce the local exciton density. The approach could be extended to electrically generated excitons, which can create highly localized exciton distributions near nanoscale contacts. Additionally, solar cells could benefit from maximizing excitation enhancement near the nanostructures while redistributing the exciton density through diffusion to reduce the loss of excitons through emission and annihilation.

Our results demonstrate the importance of tailoring nanophotonic structures to specific exciton dynamics for maximal performance. As several excitonic materials consist of nano- or microcrystals exhibiting nanophotonic resonances, their photonic properties also have implications for understanding and quantifying exciton dynamics in nanomaterials. The operation principles and limiting regimes that we provide for diffusion and annihilation in nanophotonic landscapes can thus guide the design of efficient and high-power devices. Our findings apply to light-emitting diodes or lasers using relevant families of semiconductors in the form of nanoparticles, nanowires, thin films, or monolayers.

Methods

Electromagnetic simulations

We perform the electromagnetic simulations using the surface integral equation (SIE) method for periodic nanostructures^{55,56}. We use the permittivities of silicon and silver from Green⁵⁷ and Johnson and Christy⁵⁸. We set a homogeneous relative permittivity $\epsilon_r = 1.5$ for the background medium as the geometric mean of air and glass to approximate the effect of a substrate. We apply a realistic rounding radius of 20 nm to the sharp edges of the nanodisks.

We treat the emitters as electric dipole sources lying on a plane 5 nm above the nanodisks. To compute the excitation enhancement F_{ex} , we illuminate the system with a plane wave under normal incidence from above or below depending on optimal excitation conditions and evaluate the electric field \mathbf{E} on the plane above the nanostructure. The excitation enhancement for dipolar emitters orientationally averaged in three dimensions is $|\mathbf{E}|^2/|\mathbf{E}_0|^2$, where \mathbf{E}_0 is the electric field in the absence of the nanostructures.

The emission enhancement F_{em} is the integral of the power radiated in all directions (θ, ϕ) , normalized to the same quantity in the absence of nanostructures. We compute the dipole radiation in a given direction (θ, ϕ) using electromagnetic reciprocity⁵⁹ by evaluating the field intensity at the location of the emitter under illumination by a plane wave incident from the same direction^{60–62}. This method assumes no absorption losses in the nanodisks that might reduce antenna radiation efficiency. The emission enhancement of a dipole depends on its orientation. We compute the average emission enhancements for emitters along all possible orientations in three dimensions, integrating total photoluminescence in all directions.

For emitters such as transition metal dichalcogenides where the dipoles are oriented in the plane, excitation enhancement requires using the in-plane projection of the electric field. Additionally, orientational averaging should then be performed in two dimensions. With these modifications, our treatment applies to two-dimensional excitonic materials as well and does not change the results qualitatively (Supporting Figure S8).

Numerical solution of exciton dynamics

To solve the non-dimensionalized exciton dynamics equation (2) numerically, we discretize the exciton density into a grid with non-dimensionalized coordinates: $n'(x'_i, y'_j)$ where $x'_i = i/2N, y'_j = j/2N$ for $(i, j) \in \{-N, \dots, N\}$. We choose the value of N in each simulation to obtain 5 nm spatial resolution. As a result of periodicity, the exciton densities are equal at opposite edges of the unit cell (indices $-N$ and N). In the limiting case of low incident power, the quadratic annihilation term vanishes, and we obtain a linear differential equation in n' .

Under continuous-wave illumination, in the steady state, we have $[F_{decay} - D'\nabla'^2] n' = F_{ex} I'$, where we have dropped the explicit spatial dependence. Taking the spatial Fourier transform,

$$\left[\tilde{F}_{decay} \circledast + D' q'^2 \right] \tilde{n}' = \tilde{F}_{ex} I' \quad (3)$$

where the quantities with a tilde (such as \tilde{n}') are Fourier transforms of the real-space quantities, $\tilde{F}_{decay} \circledast$ is the circular convolution matrix for \tilde{F}_{decay} , and the matrix q'^2 is the squared momentum in the Fourier transform of the discrete Laplace operator, with elements $q'_{l,m} = 4\pi^2(l^2 + m^2)$. Inverting the matrix on the left-hand side of Equation (3) gives the steady-state exciton density. Its eigenvalues describe the time evolution under pulsed illumination, providing the total decay rate enhancement.

In the presence of annihilation, we can no longer use linear methods. Hence we let the system evolve explicitly according to Equation (2) using the forward Euler method until $T = 10\tau_0$. Under continuous-wave illumination, the system reaches a steady state by this time. We model pulsed excitation using an ultrashort impulse $I'\delta(t')$ so that the exciton density instantaneously becomes $n'(\mathbf{r}', 0) = F_{ex}(\mathbf{r}')I'$. We ensure that the high initial decay rates do not result in numerical errors by using an adaptive time step that limits the maximum relative change in exciton density at a location within a time step to one percent. The total photoluminescence from the unit cell is then

$$\text{PL} = \eta_0 \iiint n'(\mathbf{r}', t') F_{em}(\mathbf{r}') dt' d\mathbf{r}'^2. \quad (4)$$

We can also calculate the decay time as the mean lifetime of emission from the temporal decay of photoluminescence:

$$\tau = \frac{\eta_0 \iiint n'(\mathbf{r}', t') F_{em}(\mathbf{r}') t' dt' d\mathbf{r}'^2}{\text{PL}}. \quad (5)$$

The total decay rate enhancement is the ratio of the decay time without the nanostructure to the average decay time in the presence of the nanostructure.

Supporting Information

Supporting Information is available from the Wiley Online Library or from the author.

Acknowledgements

We thank Rasmus H. Godiksen for illuminating discussions. This work was financially supported by the Netherlands Organization for Scientific Research (NWO) through Gravitation grant “Research Centre for Integrated Nanophotonics” (024.002.033), START-UP grant (740.018.009), and Innovational Research Incentives Scheme (VICI Grant nr. 680-47-628). S. Wang was supported by Priority Academic Program Development (PAPD) of Jiangsu Higher Education Institutions. Simulations in this work were carried out on the Dutch national e-infrastructure with the support of SURF Cooperative.

Conflict of interest

The authors declare that they have no conflict of interest.

References

- (1) Bidault, S.; Mivelle, M.; Bonod, N. Dielectric nanoantennas to manipulate solid-state light emission. *J. Appl. Phys.* **2019**, *126*, 094104.
- (2) Tiguntseva, E. Y.; Zograf, G. P.; Komissarenko, F. E.; Zuev, D. A.; Zakhidov, A. A.; Makarov, S. V.; Kivshar, Y. S. Light-Emitting Halide Perovskite Nanoantennas. *Nano Lett.* **2018**, *18*, 1185–1190.
- (3) Rutckaia, V.; Heyroth, F.; Novikov, A.; Shaleev, M.; Petrov, M.; Schilling, J. Quantum Dot Emission Driven by Mie Resonances in Silicon Nanostructures. *Nano Lett.* **2017**, *17*, 6886–6892.
- (4) Bucher, T.; Vaskin, A.; Mupparapu, R.; Löchner, F. J. F.; George, A.; Chong, K. E.;

- Fasold, S.; Neumann, C.; Choi, D.-Y.; Eilenberger, F.; Setzpfandt, F.; Kivshar, Y. S.; Pertsch, T.; Turchanin, A.; Staude, I. Tailoring Photoluminescence from MoS₂ Monolayers by Mie-Resonant Metasurfaces. *ACS Photonics* **2019**, *6*, 1002–1009.
- (5) Raziman, T. V.; Godiksen, R. H.; Müller, M. A.; Curto, A. G. Conditions for Enhancing Chiral Nanophotonics near Achiral Nanoparticles. *ACS Photonics* **2019**, *6*, 2583–2589.
- (6) Murai, S.; Castellanos, G. W.; Raziman, T. V.; Curto, A. G.; Gómez Rivas, J. Enhanced Light Emission by Magnetic and Electric Resonances in Dielectric Metasurfaces. *Adv. Opt. Mater.* **2020**, *n/a*, 1902024.
- (7) Cihan, A. F.; Curto, A. G.; Raza, S.; Kik, P. G.; Brongersma, M. L. Silicon Mie resonators for highly directional light emission from monolayer MoS₂. *Nat. Photon.* **2018**, *12*, 284–290.
- (8) Farahani, J. N.; Pohl, D. W.; Eisler, H.-J.; Hecht, B. Single Quantum Dot Coupled to a Scanning Optical Antenna: A Tunable Superemitter. *Phys. Rev. Lett.* **2005**, *95*, 017402.
- (9) Anger, P.; Bharadwaj, P.; Novotny, L. Enhancement and Quenching of Single-Molecule Fluorescence. *Phys. Rev. Lett.* **2006**, *96*, 113002.
- (10) Kühn, S.; Håkanson, U.; Rogobete, L.; Sandoghdar, V. Enhancement of Single-Molecule Fluorescence Using a Gold Nanoparticle as an Optical Nanoantenna. *Phys. Rev. Lett.* **2006**, *97*, 017402.
- (11) Vecchi, G.; Giannini, V.; Gómez Rivas, J. Shaping the Fluorescent Emission by Lattice Resonances in Plasmonic Crystals of Nanoantennas. *Phys. Rev. Lett.* **2009**, *102*, 146807.
- (12) Curto, A. G.; Volpe, G.; Taminiau, T. H.; Kreuzer, M. P.; Quidant, R.; van Hulst, N. F. Unidirectional Emission of a Quantum Dot Coupled to a Nanoantenna. *Science* **2010**, *329*, 930–933.

- (13) Huang, K. C. Y.; Seo, M.-K.; Huo, Y.; Sarmiento, T.; Harris, J. S.; Brongersma, M. L. Antenna electrodes for controlling electroluminescence. *Nat. Commun.* **2012**, *3*, 1–6.
- (14) Mohammadi, A.; Sandoghdar, V.; Agio, M. Gold nanorods and nanospheroids for enhancing spontaneous emission. *New J. Phys.* **2008**, *10*, 105015.
- (15) Novotny, L.; Hecht, B. *Principles of Nano-Optics*, 2nd ed.; Cambridge University Press, 2012.
- (16) Stranks, S. D.; Eperon, G. E.; Grancini, G.; Menelaou, C.; Alcocer, M. J. P.; Leijtens, T.; Herz, L. M.; Petrozza, A.; Snaith, H. J. Electron-Hole Diffusion Lengths Exceeding 1 Micrometer in an Organometal Trihalide Perovskite Absorber. *Science* **2013**, *342*, 341–344.
- (17) Yao, E.-P.; Bohn, B. J.; Tong, Y.; Huang, H.; Polavarapu, L.; Feldmann, J. Exciton Diffusion Lengths and Dissociation Rates in CsPbBr₃ Nanocrystal–Fullerene Composites: Layer-by-Layer versus Blend Structures. *Adv. Opt. Mater.* **2019**, *7*, 1801776.
- (18) Deng, S.; Shi, E.; Yuan, L.; Jin, L.; Dou, L.; Huang, L. Long-range exciton transport and slow annihilation in two-dimensional hybrid perovskites. *Nat. Commun.* **2020**, *11*, 1–8.
- (19) Kumar, N.; Cui, Q.; Ceballos, F.; He, D.; Wang, Y.; Zhao, H. Exciton diffusion in monolayer and bulk MoSe₂. *Nanoscale* **2014**, *6*, 4915–4919.
- (20) Yuan, L.; Wang, T.; Zhu, T.; Zhou, M.; Huang, L. Exciton Dynamics, Transport, and Annihilation in Atomically Thin Two-Dimensional Semiconductors. *J. Phys. Chem. Lett.* **2017**, *8*, 3371–3379.
- (21) Akselrod, G. M.; Prins, F.; Poulikakos, L. V.; Lee, E. M. Y.; Weidman, M. C.; Mork, A. J.; Willard, A. P.; Bulović, V.; Tisdale, W. A. Subdiffusive Exciton Transport in Quantum Dot Solids. *Nano Lett.* **2014**, *14*, 3556–3562.

- (22) Lee, E. M. Y.; Tisdale, W. A. Determination of Exciton Diffusion Length by Transient Photoluminescence Quenching and Its Application to Quantum Dot Films. *J. Phys. Chem. C* **2015**, *119*, 9005–9015.
- (23) Mikhnenko, O. V.; Blom, P. W. M.; Nguyen, T.-Q. Exciton diffusion in organic semiconductors. *Energy Environ. Sci.* **2015**, *8*, 1867–1888.
- (24) Cognet, L.; Tsybouski, D. A.; Rocha, J.-D. R.; Doyle, C. D.; Tour, J. M.; Weisman, R. B. Stepwise Quenching of Exciton Fluorescence in Carbon Nanotubes by Single-Molecule Reactions. *Science* **2007**, *316*, 1465–1468.
- (25) Amori, A. R.; Hou, Z.; Krauss, T. D. Excitons in Single-Walled Carbon Nanotubes and Their Dynamics. *Annu. Rev. Phys. Chem.* **2018**, *69*, 81–99.
- (26) Hertel, T.; Himmelein, S.; Ackermann, T.; Stich, D.; Crochet, J. Diffusion Limited Photoluminescence Quantum Yields in 1-D Semiconductors: Single-Wall Carbon Nanotubes. *ACS Nano* **2010**, *4*, 7161–7168.
- (27) Li, W.; Yadavalli, S. K.; Lizarazo-Ferro, D.; Chen, M.; Zhou, Y.; Padture, N. P.; Zia, R. Subgrain Special Boundaries in Halide Perovskite Thin Films Restrict Carrier Diffusion. *ACS Energy Lett.* **2018**, *3*, 2669–2670.
- (28) Snaider, J. M.; Guo, Z.; Wang, T.; Yang, M.; Yuan, L.; Zhu, K.; Huang, L. Ultrafast Imaging of Carrier Transport across Grain Boundaries in Hybrid Perovskite Thin Films. *ACS Energy Lett.* **2018**, *3*, 1402–1408.
- (29) Goodman, A. J.; Lien, D.-H.; Ahn, G. H.; Spiegel, L. L.; Amani, M.; Willard, A. P.; Javey, A.; Tisdale, W. A. Substrate-Dependent Exciton Diffusion and Annihilation in Chemically Treated MoS₂ and WS₂. *J. Phys. Chem. C* **2020**,
- (30) Yuan, L.; Huang, L. Exciton dynamics and annihilation in WS₂ 2D semiconductors. *Nanoscale* **2015**, *7*, 7402–7408.

- (31) Sun, D.; Rao, Y.; Reider, G. A.; Chen, G.; You, Y.; Brézin, L.; Harutyunyan, A. R.; Heinz, T. F. Observation of Rapid Exciton–Exciton Annihilation in Monolayer Molybdenum Disulfide. *Nano Lett.* **2014**, *14*, 5625–5629.
- (32) Mouri, S.; Miyauchi, Y.; Toh, M.; Zhao, W.; Eda, G.; Matsuda, K. Nonlinear photoluminescence in atomically thin layered WSe₂ arising from diffusion-assisted exciton-exciton annihilation. *Phys. Rev. B* **2014**, *90*, 155449.
- (33) Yu, Y.; Yu, Y.; Xu, C.; Barrette, A.; Gundogdu, K.; Cao, L. Fundamental limits of exciton-exciton annihilation for light emission in transition metal dichalcogenide monolayers. *Phys. Rev. B* **2016**, *93*, 201111.
- (34) Raziman, T. V.; Martin, O. J. F. Orientation Dependence of Plasmonically Enhanced Spontaneous Emission. *J. Phys. Chem. C* **2016**, *120*, 21037–21046.
- (35) Sun, G.; Khurgin, J. B.; Soref, R. A. Practical enhancement of photoluminescence by metal nanoparticles. *Appl. Phys. Lett.* **2009**, *94*, 101103.
- (36) Kinkhabwala, A.; Yu, Z.; Fan, S.; Avlasevich, Y.; Müllen, K.; Moerner, W. E. Large single-molecule fluorescence enhancements produced by a bowtie nanoantenna. *Nat. Photonics* **2009**, *3*, 654–657.
- (37) Mey, O.; Wall, F.; Schneider, L. M.; Günder, D.; Walla, F.; Soltani, A.; Roskos, H.; Yao, N.; Qing, P.; Fang, W.; Rahimi-Iman, A. Enhancement of the Monolayer Tungsten Disulfide Exciton Photoluminescence with a Two-Dimensional Material/Air/Gallium Phosphide In-Plane Microcavity. *ACS Nano* **2019**, *13*, 5259–5267.
- (38) Sortino, L.; Zotev, P. G.; Mignuzzi, S.; Cambiasso, J.; Schmidt, D.; Genco, A.; Aßmann, M.; Bayer, M.; Maier, S. A.; Sapienza, R.; Tartakovskii, A. I. Enhanced light-matter interaction in an atomically thin semiconductor coupled with dielectric nanoantennas. *Nat. Commun.* **2019**, *10*, 5119.

- (39) Hoshi, Y.; Kuroda, T.; Okada, M.; Moriya, R.; Masubuchi, S.; Watanabe, K.; Taniguchi, T.; Kitaura, R.; Machida, T. Suppression of exciton-exciton annihilation in tungsten disulfide monolayers encapsulated by hexagonal boron nitrides. *Phys. Rev. B* **2017**, *95*, 241403.
- (40) Schneider, L. M.; Lippert, S.; Kuhnert, J.; Ajayi, O.; Renaud, D.; Firoozabadi, S.; Ngo, Q.; Guo, R.; Kim, Y. D.; Heimbrodtt, W.; Hone, J. C.; Rahimi-Iman, A. The influence of the environment on monolayer tungsten diselenide photoluminescence. *Nano-Structures & Nano-Objects* **2018**, *15*, 84–97.
- (41) Fu, Y.; He, D.; He, J.; Bian, A.; Zhang, L.; Liu, S.; Wang, Y.; Zhao, H. Effect of Dielectric Environment on Excitonic Dynamics in Monolayer WS₂. *Adv. Mater. Interf.* **2019**, *6*, 1901307.
- (42) Rhodes, D.; Chae, S. H.; Ribeiro-Palau, R.; Hone, J. Disorder in van der Waals heterostructures of 2D materials. *Nat. Mater.* **2019**, *18*, 541–549.
- (43) Godiksen, R. H.; Wang, S.; Raziman, T. V.; Guimaraes, M. H. D.; Rivas, J. G.; Curto, A. G. Correlated Exciton Fluctuations in a Two-Dimensional Semiconductor on a Metal. *Nano Lett.* **2020**, *20*, 4829–4836.
- (44) Kulig, M.; Zipfel, J.; Nagler, P.; Blanter, S.; Schüller, C.; Korn, T.; Paradiso, N.; Glazov, M. M.; Chernikov, A. Exciton Diffusion and Halo Effects in Monolayer Semiconductors. *Phys. Rev. Lett.* **2018**, *120*, 207401.
- (45) Glazov, M. M. Phonon wind and drag of excitons in monolayer semiconductors. *Phys. Rev. B* **2019**, *100*, 045426.
- (46) Perea-Causín, R.; Brem, S.; Rosati, R.; Jago, R.; Kulig, M.; Ziegler, J. D.; Zipfel, J.; Chernikov, A.; Malic, E. Exciton Propagation and Halo Formation in Two-Dimensional Materials. *Nano Lett.* **2019**, *19*, 7317–7323.

- (47) Najafi, E.; Ivanov, V.; Zewail, A.; Bernardi, M. Super-diffusion of excited carriers in semiconductors. *Nat. Commun.* **2017**, *8*.
- (48) Flekkøy, E. G.; Hansen, A.; Baldelli, B. Hyperballistic Superdiffusion and Explosive Solutions to the Non-Linear Diffusion Equation. *Frontiers in Physics* **2021**, *9*.
- (49) Berghuis, A. M.; Raziman, T. V.; Halpin, A.; Wang, S.; Curto, A. G.; Rivas, J. G. Effective Negative Diffusion of Singlet Excitons in Organic Semiconductors. *J. Phys. Chem. Lett.* **2021**, *12*, 1360–1366.
- (50) Kern, A. M.; Meixner, A. J.; Martin, O. J. F. Molecule-Dependent Plasmonic Enhancement of Fluorescence and Raman Scattering near Realistic Nanostructures. *ACS Nano* **2012**, *6*, 9828–9836.
- (51) Castellanos-Gomez, A.; Roldán, R.; Cappelluti, E.; Buscema, M.; Guinea, F.; van der Zant, H. S. J.; Steele, G. A. Local Strain Engineering in Atomically Thin MoS₂. *Nano Lett.* **2013**, *13*, 5361–5366.
- (52) Liu, X.; Guo, W. Shear strain tunable exciton dynamics in two-dimensional semiconductors. *Phys. Rev. B* **2019**, *99*, 035401.
- (53) Moon, H.; Grosso, G.; Chakraborty, C.; Peng, C.; Taniguchi, T.; Watanabe, K.; Englund, D. Dynamic exciton funneling by local strain control in a monolayer semiconductor. *arXiv:1906.10077 [cond-mat]* **2019**,
- (54) Sortino, L.; Brooks, M.; Zotev, P. G.; Genco, A.; Cambiasso, J.; Mignuzzi, S.; Maier, S. A.; Burkard, G.; Sapienza, R.; Tartakovskii, A. I. Dielectric Nanoantennas for Strain Engineering in Atomically Thin Two-Dimensional Semiconductors. *ACS Photonics* **2020**, *7*, 2413–2422.
- (55) Gallinet, B.; Kern, A. M.; Martin, O. J. F. Accurate and versatile modeling of elec-

- tromagnetic scattering on periodic nanostructures with a surface integral approach. *J. Opt. Soc. Am. A* **2010**, *27*, 2261–2271.
- (56) Raziman, T. V.; Somerville, W. R. C.; Martin, O. J. F.; Le Ru, E. C. Accuracy of surface integral equation matrix elements in plasmonic calculations. *J. Opt. Soc. Am. B* **2015**, *32*, 485–492.
- (57) Green, M. A. Self-consistent optical parameters of intrinsic silicon at 300K including temperature coefficients. *Sol. Energy Mater. Sol. Cells* **2008**, *92*, 1305–1310.
- (58) Johnson, P. B.; Christy, R. W. Optical Constants of the Noble Metals. *Phys. Rev. B* **1972**, *6*, 4370–4379.
- (59) Chew, W. C. *Waves and Fields in Inhomogeneous Media*; Van Nostrand Reinhold, 1990.
- (60) Anttu, N. Modifying the emission of light from a semiconductor nanowire array. *J. Appl. Phys.* **2016**, *120*, 043108.
- (61) Kivisaari, P.; Chen, Y.; Anttu, N. Emission enhancement, light extraction and carrier dynamics in InGaAs/GaAs nanowire arrays. *Nano Futures* **2018**, *2*, 015001.
- (62) Vaskin, A.; Bohn, J.; Chong, K. E.; Bucher, T.; Zilk, M.; Choi, D.-Y.; Neshev, D. N.; Kivshar, Y. S.; Pertsch, T.; Staude, I. Directional and Spectral Shaping of Light Emission with Mie-Resonant Silicon Nanoantenna Arrays. *ACS Photonics* **2018**, *5*, 1359–1364.

Supporting Information

Exciton diffusion and annihilation in nanophotonic Purcell landscapes

T. V. Raziman,[†] C. Peter Visser,[†] Shaojun Wang,^{†,‡} Jaime Gómez Rivas,[†] and
Alberto G. Curto^{*,†}

[†]*Department of Applied Physics and Institute for Photonic Integration, Eindhoven
University of Technology, Eindhoven, The Netherlands*

[‡]*MOE Key Laboratory of Modern Optical Technologies and Jiangsu Key Laboratory of
Advanced Optical Manufacturing Technologies, School of Optoelectronic Science and
Engineering, Soochow University, Suzhou 215006, China*

E-mail: A.G.Curto@TUE.nl, Phone: +31-40-247-4205

S1 Analytical solution of the non-dimensionalized ex- citon dynamics equation for limiting cases

In the low incident power limit $I' \rightarrow 0$, both continuous and pulsed excitation result in equal enhancement factors because the superposition principle applies due to linearity. Under continuous illumination and in the absence of diffusion ($D' = 0$), we have the exciton density in the steady state

$$n'(\mathbf{r}'; I' \rightarrow 0, D' = 0) = I' \frac{F_{ex}(\mathbf{r}')}{F_{decay}(\mathbf{r}', \eta_0)}.$$

The photoluminescence is then

$$\text{PL}(\mathbf{r}'; I' \rightarrow 0, D' = 0) = \eta_0 I' \frac{F_{ex}(\mathbf{r}') F_{em}(\mathbf{r}')}{F_{decay}(\mathbf{r}', \eta_0)}.$$

By spatially averaging the photoluminescence in the unit cell and normalizing by its value in the absence of enhancements, we obtain the photoluminescence enhancement

$$F_{tot}(I' \rightarrow 0, D' = 0) = \left\langle \frac{F_{ex}(\mathbf{r}') F_{em}(\mathbf{r}')}{F_{decay}(\mathbf{r}', \eta_0)} \right\rangle. \quad (\text{S1})$$

Under the limiting cases of quantum yield ($\eta_0 \rightarrow 0$) and $\eta_0 = 1$, this expression reduces to $\langle F_{ex}(\mathbf{r}') F_{em}(\mathbf{r}') \rangle$ and $\langle F_{ex}(\mathbf{r}') \rangle$, respectively.

In the infinite diffusion limit ($D' \rightarrow \infty$), the $F_{ex}(\mathbf{r}') I'$ excitons immediately migrate through the unit cell making the exciton density uniform. Similarly, diffusion smoothens out any variations due to unequal decay rates. Hence, the exciton density becomes

$$n'(\mathbf{r}'; I' \rightarrow 0, D' \rightarrow \infty) = I' \frac{\langle F_{ex}(\mathbf{r}') \rangle}{\langle F_{decay}(\mathbf{r}', \eta_0) \rangle},$$

giving the total photoluminescence enhancement

$$F_{tot}(I' \rightarrow 0, D' \rightarrow \infty) = \frac{\langle F_{ex}(\mathbf{r}') \rangle \langle F_{em}(\mathbf{r}') \rangle}{\langle F_{decay}(\mathbf{r}', \eta_0) \rangle}. \quad (\text{S2})$$

Under the limiting cases of quantum yield $\eta_0 \rightarrow 0$ and $\eta_0 = 1$, we obtain total enhancements $\langle F_{ex}(\mathbf{r}') \rangle \langle F_{em}(\mathbf{r}') \rangle$ and $\langle F_{ex}(\mathbf{r}') \rangle$, respectively.

At high incident powers for which annihilation becomes significant, we need to retain the quadratic term. Under continuous-wave illumination and in the absence of diffusion, in the steady state we have

$$n'^2(\mathbf{r}'; D' = 0; \text{CW}) + F_{decay}(\mathbf{r}', \eta_0) n'(\mathbf{r}') - F_{ex}(\mathbf{r}') I' = 0,$$

from which we can solve for $n'(\mathbf{r}', t')$

$$n'(\mathbf{r}'; D' = 0; \text{CW}) = \frac{\sqrt{F_{decay}(\mathbf{r}', \eta_0)^2 + 4I'F_{ex}(\mathbf{r}') - F_{decay}(\mathbf{r}', \eta_0)}}{2}.$$

In the limiting case of very high incident power ($I' \rightarrow \infty$), where exciton-exciton annihilation dominates emission and non-radiative decay, we have

$$n'(\mathbf{r}'; I' \rightarrow \infty, D' = 0; \text{CW}) = \sqrt{I'F_{ex}(\mathbf{r}')},$$

giving a total photoluminescence enhancement independent of quantum yield

$$F_{tot}(I' \rightarrow \infty, D' = 0; \text{CW}) = \left\langle \sqrt{F_{ex}(\mathbf{r}')} F_{em}(\mathbf{r}) \right\rangle. \quad (\text{S3})$$

The limit of infinite diffusion ($D' \rightarrow \infty$) follows from similar arguments as before,

$$F_{tot}(I' \rightarrow \infty, D' \rightarrow \infty; \text{CW}) = \left\langle \sqrt{F_{ex}(\mathbf{r}')} \right\rangle \left\langle F_{em}(\mathbf{r}) \right\rangle. \quad (\text{S4})$$

Under pulsed illumination, we have an initial exciton density $n'(\mathbf{r}', 0) = F_{ex}(\mathbf{r}')I'$. Solving the non-dimensionalized exciton dynamics equation analytically for this initial condition under zero diffusion yields^{S1}

$$n'(\mathbf{r}', t'; I' \rightarrow \infty, D' = 0; \text{pulsed}) = \frac{F_{decay}(\mathbf{r}', \eta_0)F_{ex}(\mathbf{r}')I' \exp[-F_{decay}(\mathbf{r}', \eta_0)t']}{F_{decay}(\mathbf{r}', \eta_0) + F_{ex}(\mathbf{r}')I' \{1 - \exp[-F_{decay}(\mathbf{r}', \eta_0)t']\}}.$$

Multiplying the exciton density with the radiative decay rate and integrating it over time gives the total photoluminescence from the pulse,

$$\text{PL}(\mathbf{r}'; I' \rightarrow \infty, D' = 0; \text{pulsed}) = F_{em}(\mathbf{r}')\eta_0 \log \left[1 + \frac{F_{ex}(\mathbf{r}')I'}{F_{decay}(\mathbf{r}', \eta_0)} \right].$$

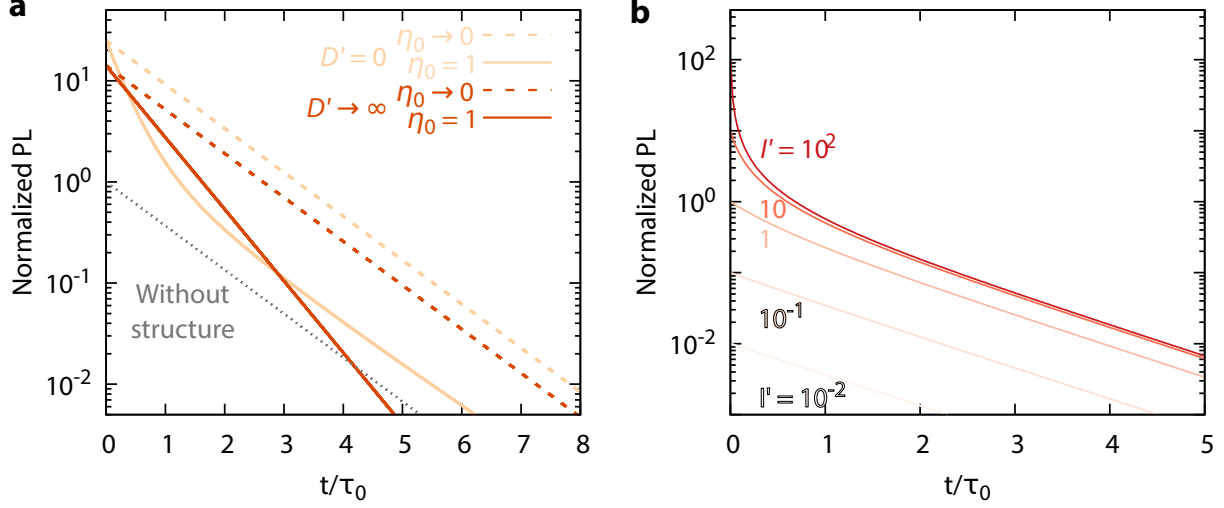


Figure S1: Exciton diffusion and annihilation modify decay rates. (a) Photoluminescence decay traces for an exciton film above the silicon nanodisk array in Figure 2a in the absence of annihilation for limits of quantum yield and diffusion. (b) Photoluminescence decay trace in the presence of annihilation for a bare exciton film with perfect quantum yield as a function of incident power.

The total photoluminescence enhancement in the limit $I' \rightarrow \infty$ is then

$$F_{tot}(I' \rightarrow \infty, D' = 0; \text{pulsed}) = \langle F_{em}(\mathbf{r}') \rangle . \quad (\text{S5})$$

The same enhancement occurs for infinite diffusion.

S2 Modification of decay rates by diffusion and annihilation

Diffusion affects the modification of decay rate when the film is placed on the nanodisk array (Figure S1a). The bare film in the absence of the nanostructure shows a mono-exponential photoluminescence decay. In the limit of ultra-low quantum yield ($\eta_0 \rightarrow \infty$), both when diffusion is very high or very low, placing the film on the nanostructure modifies only the intensity of photoluminescence but not the decay rate. This is because in this limit, the

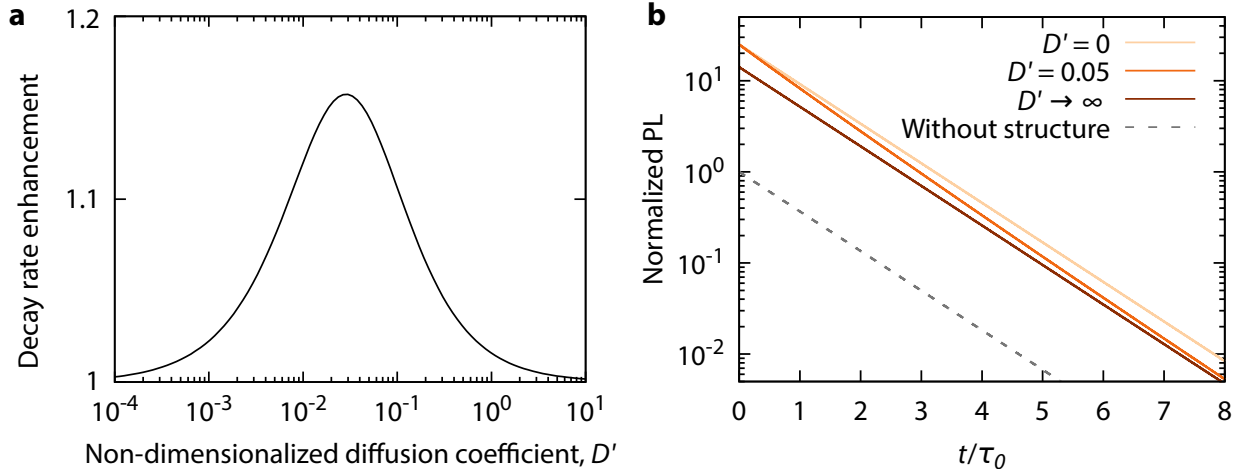


Figure S2: Diffusion modifies the decay rate of excitons near nanostructures even in the limit of ultra-low quantum yield. (a) Decay rate enhancement in the limit of ultra-low quantum yield, and (b) photoluminescence decay for different values of diffusion, for emitters above the array of silicon nanodisks in Figure 3a.

local decay rate enhancement $F_{decay} = \eta_0 F_{em} + 1 - \eta_0 \rightarrow 1$. As a result, the slope of the photoluminescence decay remains the same on the array. However, for excitons with high quantum yield, the decay rate changes on the array. In the absence of diffusion, the emitters at different locations decay with different rates, resulting in photoluminescence decay which is no longer mono-exponential. In the limit of infinite diffusion, the instant redistribution of exciton density makes the decay mono-exponential again. The increased decay rate results, however, in a different slope compared to the bare exciton film.

Exciton-exciton annihilation modifies the decay rate at high exciton densities even in the absence of nanostructures (Figure S1b). At low incident powers, the photoluminescence decay is mono-exponential because low exciton densities make annihilation negligible. As the incident power increases, annihilation results in significant decay at short time scales.

S3 Decay rate modification in the limit of ultra-low quantum yield due to diffusion

In the presence of diffusion, even the decay rates of emitters with ultra-low quantum yield change near nanostructures (Figure S2a). Both in the limit of very low and very high diffusion, there is no decay rate enhancement, as previously seen – it is only in the intermediate diffusion regime that we observe a modification of decay rate. The reason is that, in the regime of intermediate diffusion, excitons move between regions of different emission enhancements in a finite time, which results in a temporal change in the slope of the photoluminescence decay curve (Figure S2b). However, both in the limits of low and high diffusion, the photoluminescence decay is mono-exponential.

S4 Spatially decoupling excitation and emission enhancements using angular dependence of emission

The array of silicon nanodisks in Figure 3b shows improved photoluminescence enhancement with diffusion because the excitation and emission enhancements are spatially decoupled (Figure S3b). The excitation and emission wavelengths are equal, $\lambda_{ex} = \lambda_{em} = 546$ nm (Figure S3a). Spatial decoupling of these enhancements occurs in spite of the wavelengths being equal because of the angular variation in the emission from different locations in the unit cell. An exciton near the corner of the unit cell (yellow dot) emits in a narrow angle in the vertical direction (Figure S3c). Meanwhile, an emitter near the edge of the disk (blue dot) emits at an angle slightly away from the vertical. This angle explains why the large emission enhancement near the edge of the disk does not result by reciprocity in an equivalent excitation enhancement under normally incident plane wave illumination from above. In the limit of ultra-low quantum yield and zero diffusion, excitons near the corner of the unit cell dominate the emission. In the limit of infinite diffusion, on the other hand,

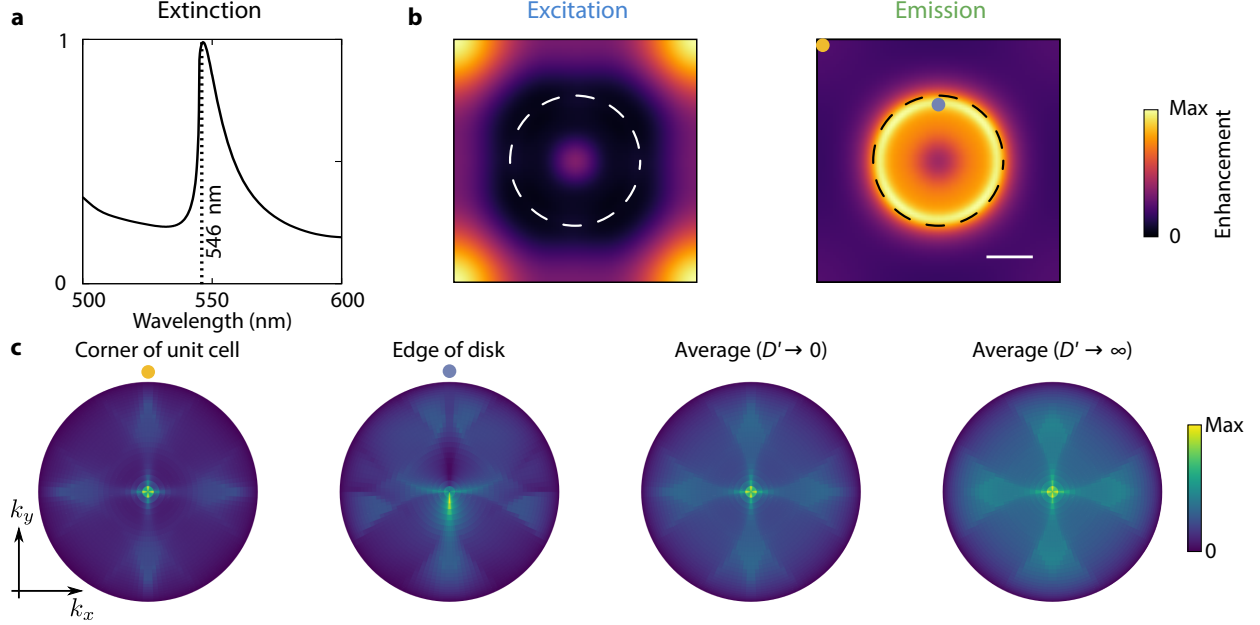


Figure S3: The angular dependence of the emission can be used to spatially decouple excitation and emission enhancements at the same wavelength. (a) Extinction of the array of silicon nanodisks in Figure 3b. (b) The maps of excitation and emission enhancements at $\lambda_{ex} = \lambda_{em} = 546$ nm for emitters above the array. Scale bar 100 nm. (c) Emission patterns in the upper half-space from excitons with ultra-low quantum yield above the array. From left to right: an emitter near the corner of the unit cell (yellow dot), an emitter near the edge of the disk (blue dot), the total emission from the film in the limit of zero diffusion, and in the limit of infinite diffusion.

excitons distribute uniformly in the unit cell before emitting. As a result, more emission away from the vertical occurs in the case of infinite diffusion.

S5 Improving photoluminescence enhancement at high power using emission-dominant enhancement

Emitters above the silver nanodisk array in Figure 6b show improved photoluminescence enhancement with increasing incident power. The array has a sharp resonance at the emission wavelength $\lambda_{em} = 600$ nm whereas the excitation wavelength $\lambda_{ex} = 450$ nm falls on a different resonance (Figure S4a). Emission enhancement of the array is higher than the excitation enhancement (Figure S4b), resulting in the nanophotonic enhancement improving at high

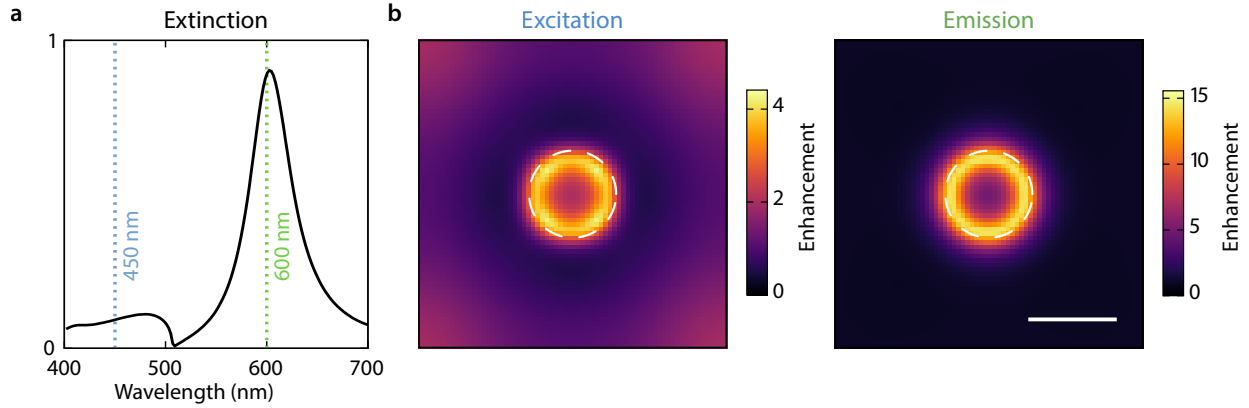


Figure S4: Nanophotonic structures with emission enhancement comparable to or higher than excitation offer improved photoluminescence enhancement with increasing power. (a) Reflectance from, and (b) maps of excitation enhancement at $\lambda_{ex} = 450$ nm and emission enhancement at $\lambda_{em} = 600$ nm above, for emitters above the array of silver nanodisks in Figure 6b. Scale bar 100 nm.

powers.

Dielectric nanostructures in which emission enhancement dominates excitation can also show improved photoluminescence enhancement at high incident powers (Figure S5).

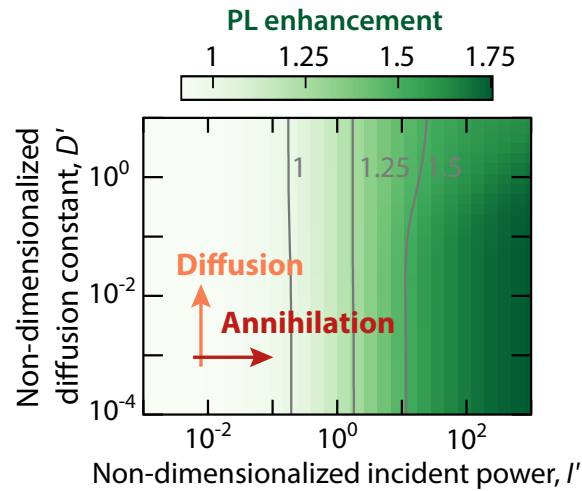


Figure S5: Dielectric nanostructures can also offer improved photoluminescence enhancement with increasing power. Photoluminescence enhancement as a function of incident power under continuous-wave illumination from above for emitters with $\eta_0 = 1$ above an array of silicon nanodisks with $R = 110$, $H = 85$, $P = 400$ nm.

Table S1: Representative reported parameters for excitonic materials. Intrinsic quantities are decay rate Γ_0 , quantum yield η_0 , diffusion constant D , annihilation constant γ , and absorption constant σ . Exciton density n_0 and incident power I_0 are the characteristic values used to non-dimensionalize the exciton dynamics equation (1). D' is the non-dimensionalized diffusion constant for period $P = 365$ nm. The quantum yield of the MoS₂ monolayer on the quartz substrate is unity due to treatment with bis(trifluoromethane)sulfonimide (TFSI).^{S2}

Material	Γ_0 (ns ⁻¹)	η_0 (%)	D (cm ² s ⁻¹)	γ (cm ² s ⁻¹)	σ (J ⁻¹)	n_0 (cm ⁻²)	I_0 (mW μm^{-2})	D'
Transition metal dichalcogenide monolayers								
WSe ₂ ^{S3}	0.25	0.1	2.2	0.35	2×10^{17}	7.1×10^8	8.9×10^{-6}	6.6
WS ₂ ^{S4,S5}	1.24	6	2	0.41	9.4×10^{16}	3×10^9	4×10^{-4}	1.2
MoSe ₂ ^{S6-S8}	7.7	0.38	12	0.165	5.2×10^{16}	4.7×10^{10}	6.8×10^{-2}	1.2
MoS ₂ ^{S2}	0.056	100	0.06	0.8	1.8×10^{17}	6.9×10^7	2.1×10^{-7}	0.81
Two-dimensional perovskites^{S9}								
1 layer	0.45	0.79	0.06	1.7×10^{-2}	2.6×10^{16}	2.6×10^{10}	4.5×10^{-3}	0.10
2 layers	0.23	0.79	0.07	4.1×10^{-3}	3.2×10^{16}	5.6×10^{10}	4.0×10^{-3}	0.23
3 layers	0.3	0.79	0.15	3.5×10^{-3}	3.5×10^{16}	8.6×10^{10}	7.3×10^{-3}	0.38
4 layers	0.2	0.79	0.25	2.8×10^{-3}	3.1×10^{16}	7.1×10^{10}	4.6×10^{-3}	0.94
5 layers	0.15	0.79	0.34	1.3×10^{-3}	3.2×10^{16}	1.2×10^{11}	5.3×10^{-3}	1.7

S6 Nanophotonic enhancement in realistic materials

Diffusion and annihilation strongly modify the photoluminescence enhancement of realistic excitonic materials in nanostructured landscapes. We tabulate the intrinsic excitonic parameters of some transition metal dichalcogenide monolayers and two-dimensional perovskites from various references in Table S1. As the sources do not provide the absorption constant σ directly, we calculate it from the absorptance by assuming that every absorbed photon generates an exciton.^{S4} Along with the intrinsic parameters, we also show the characteristic exciton density n_0 and the characteristic power I_0 used for non-dimensionalization, as well as the non-dimensionalized diffusion constant D' for $P = 365$ nm.

The non-dimensionalized diffusion constants for all the TMD monolayers are of the order of unity (Table S1). As a result, the silicon array in Figure 4c optimized for highly diffusive excitons provides strong photoluminescence enhancement for TMD monolayers with low

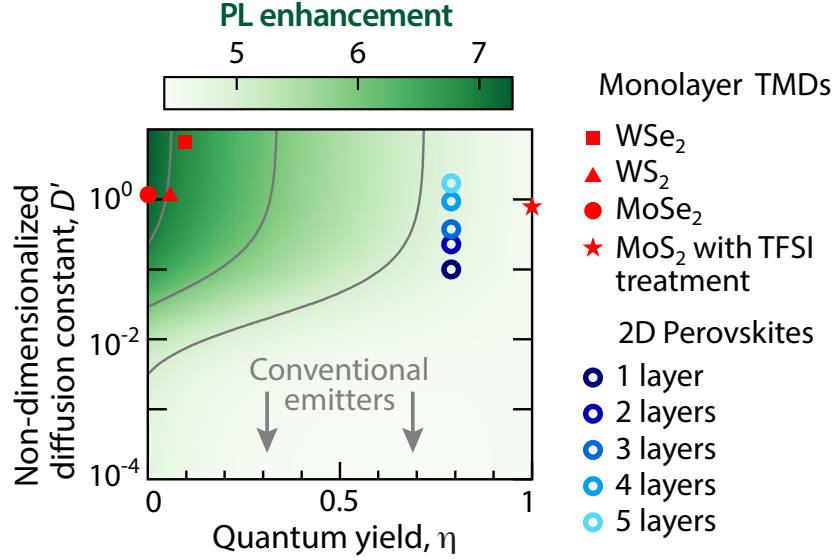


Figure S6: Realistic excitonic materials are highly diffusive, which modifies their photoluminescence enhancement. Excitonic parameters for TMD monolayers and 2D perovskites, overlaid on the photoluminescence enhancement of the array of silicon nanodisks (Figure 4c).

quantum yield (Figure S6). Treating the excitons as conventional immobile emitters would significantly underestimate their photoluminescence enhancement in this case. Emitters with high quantum yield such as 2D perovskites and TFSI-treated MoS₂ do not see a significant modification of photoluminescence enhancement on account of their high diffusion.

Typical excitonic emitters with high quantum yield also suffer from strong exciton-exciton annihilation (Table S1). Due to the low intrinsic decay rate and high annihilation in MoS₂ monolayers treated with TFSI, annihilation effects become significant at very low powers of the order of a few nW/ μm^2 (Figure S7). At typical powers of the order of $\mu\text{W}/\mu\text{m}^2$, the silver nanodisk array in Figure 6b designed to be emission dominant shows high photoluminescence enhancement. Monolayers of 2D perovskites show much lower annihilation, which nevertheless becomes significant at high powers of the order of mW/ μm^2 . The interplay between diffusion and annihilation also becomes relevant at intermediate powers for both materials due to their high non-dimensionalized diffusion constants.

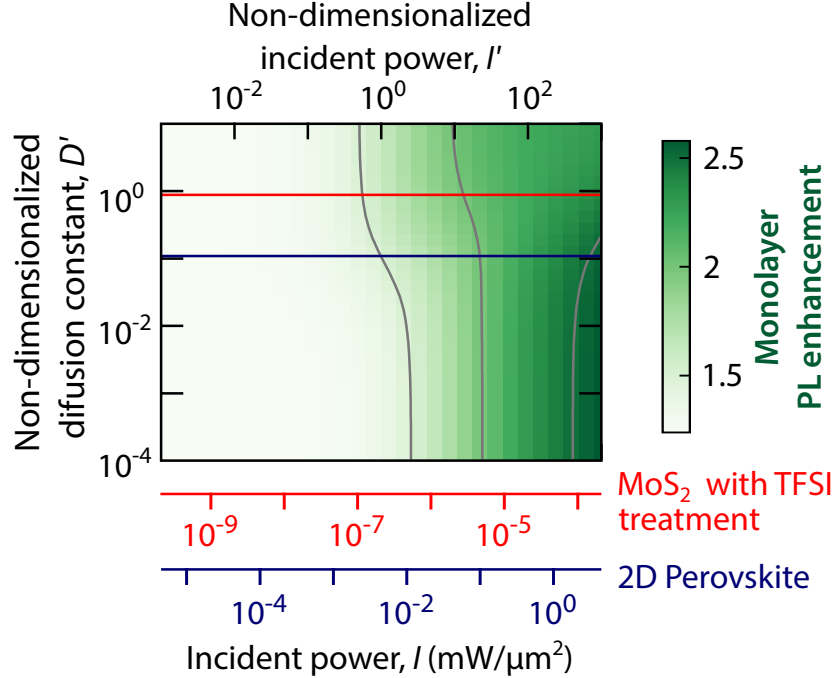


Figure S7: Realistic excitonic materials with high quantum yield show annihilation at typical illumination powers. Photoluminescence enhancement of the array of silver nanodisks (Figure 6b), overlaid with the illumination powers (I) of monolayers of MoS₂ and 2D perovskites, corresponding to the non-dimensionalized incident power I' .

S7 Dimensionality of emitter orientations

As excitons in typical materials do not have a preferential orientation, we compute the average excitation enhancement in the main text from the total electric field intensity (see Methods). Similarly, we computed the emission enhancement by averaging emitters along all possible orientations in three dimensions. However, the direct transitions in TMD monolayers occur through in-plane electric fields only. As a result, their excitation enhancement only depends on the in-plane electric field intensity^{S10} and their emission enhancement will be the average enhancement of dipoles along all two-dimensional orientations.

Although the dimensionality changes the numerical value of enhancements, the qualitative behavior remains the same (Figure S8). Physical effects we discussed in the main text such as diffusion decoupling excitation and emission enhancements and annihilation suppressing the relevance of excitation are independent of the whether we consider two-dimensional

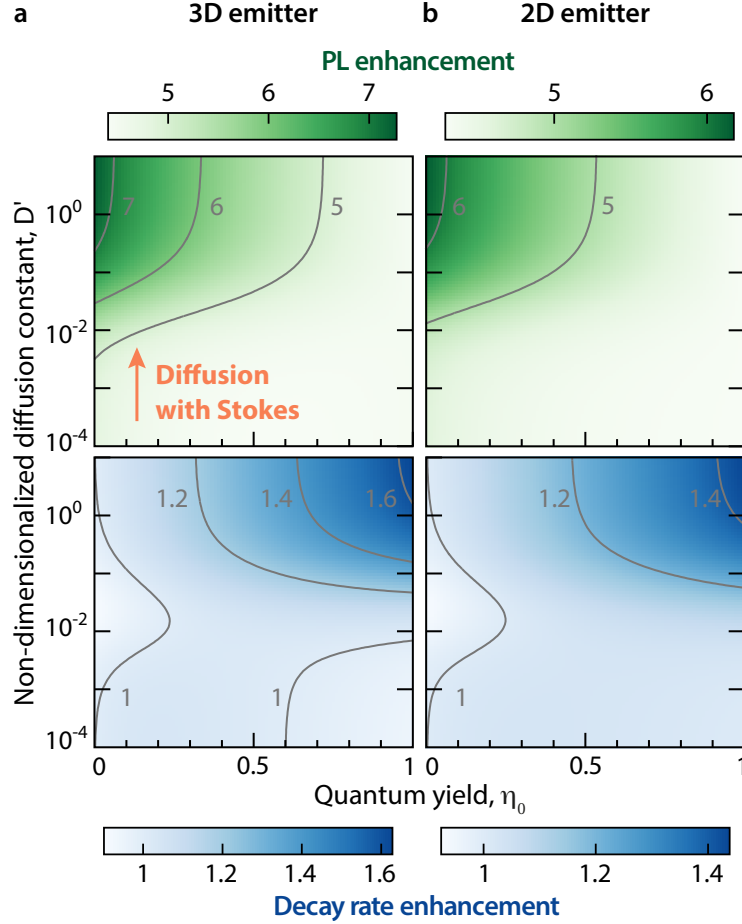


Figure S8: Nanophotonic enhancements of dipolar emitters orientationally averaged in two dimensions have a similar qualitative dependence with exciton dynamics as emitters orientationally averaged in three dimensions. Enhancements of photoluminescence and total decay rate under excitation at $\lambda_{ex} = 461$ nm and emission at $\lambda_{em} = 553$ nm for the silicon nanodisk array in Figure 3a for emitters orientationally averaged in (a) three dimensions (corresponding to Figure 4c), and (b) in two dimensions.

or three-dimensional emitters.

S8 Emission enhancement counteracts diffusion

In systems with high emission enhancement, the reduced lifetime of the exciton lowers the effective diffusion length as well. As a result, increasing the emission enhancement can turn an emitter in the $D' \rightarrow \infty$ limit to one in the $D' \rightarrow 0$ limit.

As an example, consider a system where excitation and emission enhancements are both

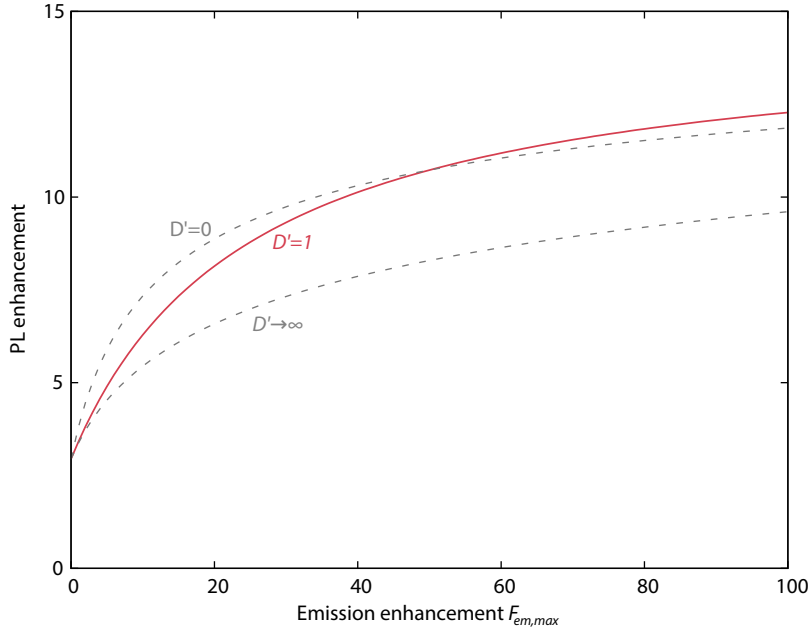


Figure S9: Increasing the emission enhancement counteracts the effect of diffusion. For an excitonic material with $D' = 1$ and $\eta_0 = 0.2$, increasing the Purcell factor takes PL enhancement from the infinite diffusion limit to the zero diffusion limit.

Gaussians at the centre of the unit cell with half-widths equal to 25% of the periodicity. We take the exciton parameters $D' = 1$ and $\eta_0 = 0.2$. Keeping the height $F_{ex,max}$ of the excitation enhancement Gaussian fixed at 10, we vary the height $F_{em,max}$ of the emission enhancement Gaussian. At low values of emission enhancement, excitons can diffuse throughout the unit cell, making the PL enhancement similar to the case of infinite diffusion (Figure S9). However, when the emission enhancement increases, the excitons decay quicker, reducing the distance they can diffuse. As a result, the PL enhancement becomes similar to the limit of zero diffusion.

S9 Photoluminescence enhancement in nanowires

Although we have discussed the interplay of exciton dynamics and nanophotonic enhancement in the context of excitonic films, the underlying principles can be extended to other geometries as well. Nanowires are ubiquitous one-dimensional excitonic structures. We con-

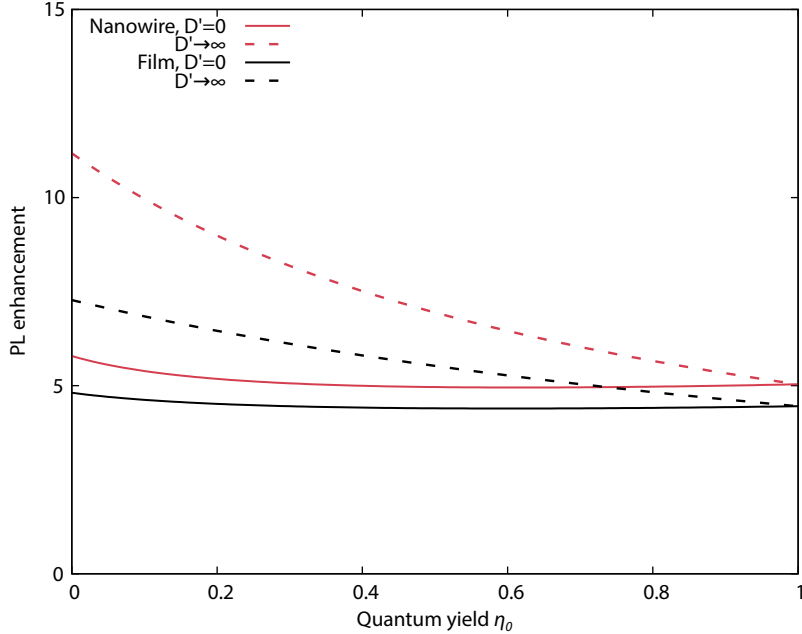


Figure S10: When the film of excitonic material above the silicon nanodisk array in Figure 3a is replaced by a long nanowire along the diagonal of the unit cell, the dependence of PL enhancement ($\lambda_{ex} = 461$ nm, $\lambda_{em} = 553$ nm) on diffusion remains the same qualitatively.

consider a long nanowire along the diagonal of the silicon nanodisk array in Figure 3a, spanning many unit cells so that we can treat it as infinitely long. We neglect scattering effects at the two ends of the nanowire and compute the PL enhancements at the zero and infinite diffusion limits for $\lambda_{ex} = 461$ nm, $\lambda_{em} = 553$ nm (corresponding to Figure 4c). As the average excitation and emission enhancements are higher on the diagonal compared to other regions (Figure 4b), PL enhancement is higher for the nanowire than the film (Figure S10). Qualitatively, both the film and the wire show similar behavior of PL enhancement increasing with diffusion and decreasing with quantum yield.

References

- [S1] Shaw, P. E.; Ruseckas, A.; Samuel, I. D. W. Exciton Diffusion Measurements in Poly(3-hexylthiophene). *Adv. Mater.* **2008**, *20*, 3516–3520.
- [S2] Goodman, A. J.; Lien, D.-H.; Ahn, G. H.; Spiegel, L. L.; Amani, M.; Willard, A. P.;

- Javey, A.; Tisdale, W. A. Substrate-Dependent Exciton Diffusion and Annihilation in Chemically Treated MoS₂ and WS₂. *J. Phys. Chem. C* **2020**,
- [S3] Mouri, S.; Miyauchi, Y.; Toh, M.; Zhao, W.; Eda, G.; Matsuda, K. Nonlinear photoluminescence in atomically thin layered WSe₂ arising from diffusion-assisted exciton-exciton annihilation. *Phys. Rev. B* **2014**, *90*, 155449.
- [S4] Yuan, L.; Huang, L. Exciton dynamics and annihilation in WS₂ 2D semiconductors. *Nanoscale* **2015**, *7*, 7402–7408.
- [S5] Yuan, L.; Wang, T.; Zhu, T.; Zhou, M.; Huang, L. Exciton Dynamics, Transport, and Annihilation in Atomically Thin Two-Dimensional Semiconductors. *J. Phys. Chem. Lett.* **2017**, *8*, 3371–3379.
- [S6] Kumar, N.; Cui, Q.; Ceballos, F.; He, D.; Wang, Y.; Zhao, H. Exciton diffusion in monolayer and bulk MoSe₂. *Nanoscale* **2014**, *6*, 4915–4919.
- [S7] Kumar, N.; Cui, Q.; Ceballos, F.; He, D.; Wang, Y.; Zhao, H. Exciton-exciton annihilation in MoSe₂ monolayers. *Phys. Rev. B* **2014**, *89*, 125427.
- [S8] Roy, S.; Sharbirin, A. S.; Lee, Y.; Kim, W. B.; Kim, T. S.; Cho, K.; Kang, K.; Jung, H. S.; Kim, J. Measurement of Quantum Yields of Monolayer TMDs Using Dye-Dispersed PMMA Thin Films. *Nanomaterials* **2020**, *10*, 1032.
- [S9] Deng, S.; Shi, E.; Yuan, L.; Jin, L.; Dou, L.; Huang, L. Long-range exciton transport and slow annihilation in two-dimensional hybrid perovskites. *Nat. Commun.* **2020**, *11*, 1–8.
- [S10] Raziman, T. V.; Godiksen, R. H.; Müller, M. A.; Curto, A. G. Conditions for Enhancing Chiral Nanophotonics near Achiral Nanoparticles. *ACS Photonics* **2019**, *6*, 2583–2589.